UGROUND: TOWARDS UNIFIED VISUAL GROUNDING WITH UNROLLED TRANSFORMERS

Anonymous authors
Paper under double-blind review

ABSTRACT

We present UGround, a **U**nified visual **Ground**ing paradigm that dynamically selects intermediate layers across **U**nrolled transformers as "mask as prompt", diverging from the prevailing pipeline that leverages the fixed last hidden layer as "`<SEG>` as prompt". UGround addresses two primary challenges posed by the prevailing paradigm: (1) its reliance on the fixed last hidden layer, which sequentially amplifies cumulative errors arising from layer-by-layer propagation without intermediate correction, and (2) its use of `<SEG>` as a prompt, which implicitly projects textual embeddings into visual space without explicit spatial cues (*e.g.*, coordinates). Central to UGround is Policy-Prompted Masking, which comprises two key components: Stochastic Skip Connection (SSC) and Mask as Prompt (MasP). SSC is a reinforcement learning policy that, via stochastic sampling, allows each `<SEG>` token to slide across unrolled transformer layers, enabling dynamic layer selection at which it connects to the vision model (*e.g.*, SAM) in a skip-connection fashion. Given the selected hidden layer, MasP uses the similarity map derived from the `<SEG>` token and image tokens as a soft logit mask to prompt SAM for mask generation, offering explicit spatial cues through its activation regions. To validate the effectiveness of UGround, we, for the first time, have unified visual grounding within a single framework from an attribute perspective, spanning from traditional refer expression segmentation to newly proposed reasoning segmentation, single-target to multi-target, positive query to false premise (empty target). All codes are provided in the supplementary material.

1 INTRODUCTION

Visual grounding aims to align referring expressions with their corresponding regions in an image or video (Mao et al., 2016; Yu et al., 2016). Despite existing efforts (Zou et al., 2023a; Liu et al., 2024b; Zou et al., 2023b; Liang et al., 2023; Liu et al., 2023; Wang et al., 2022), it remains largely unexplored under the newly emerging task settings (Lai et al., 2024; Wu et al., 2024; Xia et al., 2024; Rasheed et al., 2024; Ren et al., 2024; Qian et al., 2025). As shown in Table 1, the shifts across recent tasks settings reveal how visual grounding has evolved, from referring to objects by an explicit mention (RES (Rasheed et al., 2024; Ren et al., 2024)) to reasoning over descriptive language in an implicit fashion (RS (Lai et al., 2024; Yang et al., 2023)); from processing single-target queries per instance to handling multi-target scenarios (gRES (Xia et al., 2024), Multi-RS (Ren et al., 2024)); and from responding solely to positive queries to rejecting false premises with empty targets (FP-RES (Wu et al., 2024; Xia et al., 2024; Qian et al., 2025)). Such shifts reflect the intrinsic properties of tasks, which we term "attribute variation".

However, we observe that little research has looked into unifying existing tasks within a single framework from an attribute perspective, diverging from prior works (Ren et al., 2024; Rasheed et al., 2024; Wei et al., 2025) that primarily focus on versatile capabilities. Generally, perception systems engaging with real-world scenarios are expected to reason over implicit instructions (cognition), interact with one or multiple targets (generality), and appropriately reject queries when necessary (safety). Built upon attribute basis described above, versatility-level extensions, such as grounding in videos (Wei et al., 2025) or conversations (Rasheed et al., 2024), find their footing. This leads us to ask: *Can we design a unified architecture to bridge this gap?*

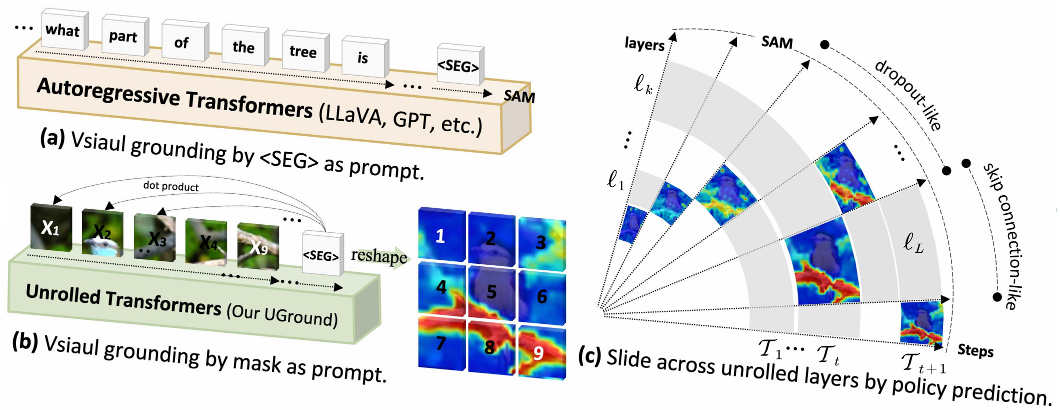
... what part of the tree is <SEG>
Autoregressive Transformers (LLaVA, GPT, etc.)
SAM
(a) Vsiaul grounding by <SEG> as prompt.
dot product
X1 X2 X3 X4 X9 <SEG>
reshape
1 2 3 4 5 6 7 8 9
Unrolled Transformers (Our UGround)
(b) Vsiaul grounding by mask as prompt.
layers
SAM
dropout-like
skip connection-like
ℓ_k
ℓ_1
ℓ_L
$\mathcal{T}_1 \cdots \mathcal{T}_t$
$\mathcal{T}_{t+1}$
Steps
(c) Slide across unrolled layers by policy prediction.

Figure 1: Prior works typically use <SEG> token embeddings from the last hidden layer as the prompt in (a). In contrast, we leverage the similarity map in Eq. (6), generated from <SEG> and image token embeddings across dynamically selected transformer layers, as the prompt in (b). Dynamic layer selection allows the similarity map to slide across transformer layers in (c). Due to the sequential nature of transformers, $\ell_L - \ell_k$ layers are skipped, enabling a direct connection with SAM in a single forward step $\mathcal{T}_t$ ("skip-connection-like"). Across multiple forward steps $\mathcal{T}_1$ to $\mathcal{T}_T$, the connectivity to SAM varies dynamically, with only one path activated at each step ("dropout-like").

Table 1: Attribute variation w.r.t. visual grounding. RES: Referring Expression Segmentation, RS: Reasoning Segmentation, FP: False Premise, gRES: Generalized RES, Multi-RS: Multi-target RS.

Method	RES	RS	FP-RES	gRES	Multi-RS
LISA (Lai et al., 2024)	✓	✓	✗	✗	✗
SESAME (Wu et al., 2024)	✓	✓	✓	✗	✗
READ (Qian et al., 2025)	✓	✓	✓	✗	✗
GLaMM (Rasheed et al., 2024)	✓	✓	✗	✓	✗
GSVA (Xia et al., 2024)	✓	✓	✓	✓	✗
PixelLM (Ren et al., 2024)	✓	✓	✗	✓	✓
UGround (Ours)	✓	✓	✓	✓	✓

Bearing this in mind, we revisit the methods of visual grounding presented in Table 1, where we identify two key challenges of the off-the-shelf models: (1) its reliance on the fixed last hidden layer, and (2) its use of <SEG> as a prompt. Current Large Multimodal Models (LMMs) based visual grounding typically leverage <SEG> token stemming from the fixed last hidden layer of the vision-language model's stacked transformers (*e.g.*, LLaVA) to prompt the downstream vision model (*e.g.*, SAM) as shown in Fig. 1(a). These stacked transformers can be deep, *e.g.*, 32 layers for LLaVA 7B, 40 layers for LLaVA 13B. In this paradigm, only the last hidden layer (layer 40) interacts with the vision SAM directly, whereas the other layers (layers 1-39) are separated. Consider telephone game by analogy, a message is passed from person to person (layer to layer) and becomes increasingly distorted before reaching the final participant (SAM). With only a single path, it sequentially amplifies cumulative errors arising from layer-by-layer propagation without any intermediate correction. In contrast to the similarity map with activation regions in Fig. 1(b), <SEG> token, a text placeholder, lacks explicit spatial cues on its own, *e.g.*, coordinates. It works via the alignment from text vocabulary into vision space in an implicit way of a fully connected layer. Inspired by the above findings, a natural idea is whether we can "cheat" this telephone game by letting the final participant (SAM) tap into intermediate layers (*e.g.*, 1–39) in advance, through "mask as prompt".

To this end, we present UGround, a **U**nified visual **Ground**ing paradigm that dynamically selects intermediate layers across **U**nrolled transformers as "mask as prompt". Central to our UGround is Policy-Prompted Masking (PPM), which consists of two key components: Stochastic Skip Connections (SSC) and Mask as Prompt (MasP). As shown in Fig. 1(c), SSC is a stochastic reinforcement learning policy that allows each <SEG> token to slide across unrolled transformer layers, reinforcing dynamic layer selection at which it connects to the vision model (*e.g.*, SAM) in a skip-connection fashion. Remarkably, SSC enables intermediate layers to skip subsequent ones and connect directly with SAM within each forward $\mathcal{T}_t$ ("skip-connection-like"). Across forward $\mathcal{T}_1$ to $\mathcal{T}_T$, such mechanism virtually connects all layers to SAM while activating only one pass at a time ("dropout-like"). Given the selected hidden layer, MasP uses the similarity map derived from the <SEG> token and image tokens as a soft logit mask to prompt SAM for mask generation, offering explicit spatial cues through its activation regions in the forward. Particularly, the similarity map is differentiable, beyond its implicit optimization via SAM backpropagation, we further impose a cross-entropy loss against the ground-truth mask to explicitly guide spatial cues in the backward. In summary, our contributions are threefold:

- We have "unified" visual grounding within a single framework from an attribute perspective. Previously, existing works either focus on explicit rather than implicit expressions, or handle single-target instead of multi-target scenarios, or respond solely to positive queries without rejecting false premises (empty target).
- We have "unrolled" stacked transformers, letting vision decoder tap into intermediate layers in a stochastic skip-connection fashion, in the way of "mask as prompt". Importantly, we explicitly supervise the prompted mask (similarity map) against the ground-truth mask to further guide the model on where to attend.
- We conduct extensive experiments on the recently proposed ReasonSeg dataset, the classic RefCOCO(+/g) dataset, and gRefCOCO(+/g). Our UGround outperforms the state of the art, achieving up to 9.0% gains in cIoU on ReasonSeg and 12.1% gains in N-acc on gRefCOCO(+/g) val sets.

2 Related Work

Large Multimodal Models. Depending on the trade-offs between computational efficiency and performance ceiling, we categorize LMMs into two groups: (1) *Fusion-centric models*, which aim for deeply fine-grained multimodal interaction by projecting visual, textual, and other modalities into a shared high-dimensional space with cross-attention mechanisms (Alayrac et al., 2022; Wang et al., 2023; Pi et al., 2023; Lv et al., 2023; Zhang et al., 2024a). Flamingo (Alayrac et al., 2022) unlocks few-shot visual reasoning by bridging a frozen language model and a vision encoder with gated cross-attention. VisionLLM (Wang et al., 2023) conditions a language model on image features via cross-attention to handle diverse vision-centric tasks, generating task-specific tokens for open-ended reasoning. GPT4RoI (Zhang et al., 2024a) enables region-of-interest (RoI) reasoning through RoI-aware cross-attention, allowing users to reference any image region in dialogue. Kosmos-2 (Peng et al., 2024) and DetGPT (Pi et al., 2023) equip LMMs with grounding capabilities. (2) *Alignment-centric models*, which employ a divide-and-conquer strategy, projecting the outputs of frozen or lightly fine-tuned unimodal encoders (*e.g.*, ViT for vision, LLaMA/GPT for text) into a shared latent space via a lightweight alignment adapter (*e.g.*, projectors, Q-Formers) (Li et al., 2023; Ye et al., 2023; Li et al., 2025; Liu et al., 2024a; Zhu et al., 2024). Otter (Li et al., 2025) instruction-tunes a Flamingo-style vision–language model on the MIMIC-IT dataset. LLaVA (Liu et al., 2024a) and MiniGPT-4 (Zhu et al., 2024) align a pretrained vision encoder with a frozen LLM using lightweight adapters for open-ended, instruction-following visual reasoning. Unlike LLaVA and MiniGPT-4, which rely on linear projections, BLIP-2 (Li et al., 2023) pioneers the Q-Former to distill visual features into compact queries for alignment with a frozen LLM. mPLUG-OWL (Ye et al., 2023) utilizes a visual abstractor to summarize global image features into condensed semantic tokens. In contrast, our UGround builds upon LLaVA (Liu et al., 2024a) for visual autoregressive modeling.

Unified Segmentation Models. Depending on the semantic granularity of joint tasks, we divide literature into two groups: *Versatility-oriented segmentation*, which aims to unify multiple functional properties within a single model (Wei et al., 2025; Cheng et al., 2022; Li et al., 2024; Zhang et al., 2024b; Bai et al., 2024; Rasheed et al., 2024), as opposed to prior works dedicated exclusively to semantic (Long & Shelhamer, 2015; Ronneberger et al., 2015; Badrinarayanan et al., 2017), instance (He et al., 2017; Liu et al., 2018; Carion et al., 2020), or panoptic segmentation (Kirillov et al., 2019b; Xiong et al., 2019; Kirillov et al., 2019a). Mask2Former (Cheng et al., 2022) pioneers a unified approach for image-level semantic, instance, and panoptic segmentation. OMG-Seg (Li et al., 2024) extends Mask2Former to their video-level counterparts. HyperSeg (Wei et al., 2025) and OMG-LLAVA (Zhang et al., 2024b) distinguish themselves from previous purely visual models (Cheng et al., 2022; Li et al., 2024) by leveraging LMMs to generate interactive text. VideoLISA (Bai et al., 2024) and HyperSeg (Wei et al., 2025) inject complex reasoning capabilities into generic video segmentation models. (2) *Attribute-oriented segmentation*, which seeks to unify the intrinsic property variations within the task itself, spanning from explicit expressions to implicit instructions, one target to many targets, and positive queries to false premises. LISA (Lai et al., 2024) elevates RES to RS by leveraging self-reasoning capabilities of LMMs. SESAME (Wu et al., 2024) and READ (Qian et al., 2025) extend LISA by rejecting false premises. GSVA (Xia et al., 2024) and PixelLM (Ren et al., 2024) generalize RES to gRES by supporting multiple targets. Closest to our work, PixelLM (Ren et al., 2024) cannot tackle empty targets, while GSVA (Xia et al., 2024) fails to handle multi-target reasoning. Attribute-oriented unification is more fundamental, as it can be applied from a versatile perspective to any specialized task. Yet, we observe that little research has looked into unifying existing tasks within a single framework from an attribute perspective, we therefore present UGround.

3 Reflection on Visual Grounding

In this section, we first revisit visual grounding with LMMs and then analyze the underlying challenges posed by the typical paradigm presented in (Lai et al., 2024; Wu et al., 2024; Qian et al., 2025).

3.1 Revisiting

Problem Definition: Let $\mathbf{x}_{img} \in \mathbb{R}^{h \times w \times c}$ denote an input image with height h, width w, and c channels, and let $\mathbf{x}_{txt}$ represent the paired textual input, which can span from an explicit mention (*e.g.*, "twigs") to an implicit description (*e.g.*, "what part of the tree"). For segmentation, visual grounding aims to generate a mask that localizes the region of $\mathbf{x}_{img}$ described by the textual query $\mathbf{x}_{txt}$ as

$$\Theta_{\mathrm{MLE}} = \arg\max_{\Theta} \mathbb{E}_{\hat{\mathbf{M}} \sim \mathcal{G}_\theta(\cdot|\mathbf{x})} \left[\log \mathcal{G}_\theta(\hat{\mathbf{M}} \mid \mathbf{x}) \right], \tag{1}$$

where $\mathbf{x}$ denotes a multimodal sequence of discrete tokens derived from $\mathbf{x}_{img}$ and $\mathbf{x}_{txt}$. $\hat{\mathbf{M}} \in \{0,1\}^{h \times w}$, 1 indicates the foreground and 0 otherwise. $\mathcal{G}_\theta$ indicates LMMs-based segmentation, including a multi-modal LLM $\mathcal{G}_\mathcal{T}$ and a visual backbone model $\mathcal{G}_\mathcal{V}$. Formally, $\mathcal{G}_\theta = \mathcal{G}_\mathcal{V} \circ \mathcal{G}_\mathcal{T}$, $\circ$ denotes the composition operation. As illustrated in Fig. 3, we use LLaVA (Liu et al., 2024a) for $\mathcal{G}_\mathcal{T}$ and SAM (Kirillov et al., 2023) for $\mathcal{G}_\mathcal{V}$, respectively.

To equip $\mathcal{G}_\theta$ with reasoning capabilities of LMMs, LISA (Lai et al., 2024) augments the text vocabulary of $\mathcal{G}_\mathcal{T}$ with a <SEG> token. Consider an input sequence $\mathbf{x} = (x_1, x_2, \ldots, x_T)$, $\mathcal{G}_\mathcal{T}$ consumes $\mathbf{x}$ as input with L stacked transformer layers, which in turn response hidden states as

$$\mathcal{H}^{(\ell)} = \mathcal{G}_\mathcal{T}^{(\ell)}\big(\mathcal{H}^{(\ell-1)}\big), \quad \ell = 1, 2, \ldots, L, \tag{2}$$

where $\mathcal{H}^{(0)}$ denotes the embeddings of the input sequence $\mathbf{x}$ at the embedding layer. The hidden state at the ℓ-th layer can be presented as $\mathcal{H}^{(\ell)} = \left\{ \boldsymbol{h}_1^{(\ell)}, \boldsymbol{h}_2^{(\ell)}, \ldots, \boldsymbol{h}_T^{(\ell)} | \boldsymbol{h}_t^{(\ell)} \in \mathbb{R}^d \right\}$. Let t^* be the position of the <SEG> token in the input sequence $\mathbf{x}$, then its corresponding hidden state at the ℓ-th layer is $\boldsymbol{h}_{t^*}^{(\ell)}$, which is finally fed into $\mathcal{G}_\mathcal{V}^{dec}$ to generate the binary segmentation mask $\hat{\mathbf{M}}$ as

$$\hat{\mathbf{M}} = \mathcal{G}_\mathcal{V}^{dec}(\mathbf{f}, \boldsymbol{h}_{seg}), \quad \boldsymbol{h}_{seg} = \varphi(\boldsymbol{h}_{t^*}^{(\ell)}) \in \mathbb{R}^d, \tag{3}$$

where $\varphi(\cdot)$ is a multilayer perceptron (MLP) projection layer, $\mathbf{f}$ is the visual features of the input image $\mathbf{x}_{img}$ extracted by the vision backbone $\mathcal{G}_\mathcal{V}^{enc}$ in SAM (Kirillov et al., 2023). However, we observe that existing works (Lai et al., 2024; Wu et al., 2024; Xia et al., 2024; Rasheed et al., 2024; Ren et al., 2024; Qian et al., 2025) predominantly utilize the embedding from the fixed last hidden layer ($\ell = L$) as the <SEG> token representation $\boldsymbol{h}_{seg}$, while the impact of intermediate layers remains largely unexplored.

3.2 Analysis

Why Dynamic Layer Selection. To analyze the impact of intermediate layers, we train UGround on the ReasonSeg *train* set with two strategies: (1) relying solely on the last hidden layer ($\ell = L$), and (2) dynamically selecting from the intermediate layers ($\ell \in \{1, \ldots, L-1\}$). Qualitatively, we visualize the similarity maps across layers 1–40 of $\mathcal{G}_\mathcal{T}$ in Fig. 4. We observe that the fixed-last-layer strategy produces noisy similarity maps in intermediate layers (Fig. 4(a)), whereas the intermediate-layer counterpart yields a more discriminative foreground (Fig. 4(b)). Quantitatively, we plot the predicted cIoU of the embeddings across layers 1–40. Fig.2(a) shows that every layer from 10–40 improves over the fixed-last-layer strategy by a clear and consistent margin. We further plot the per-layer similarity-map loss with respect to the ground-truth mask. Fig.2(b) shows that the intermediate-layer strategy begins converging from layer 19 and ultimately reaches a lower loss level, while the fixed-last-layer strategy only starts converging from layer 28, indicating that dynamic layer selection accelerates convergence.

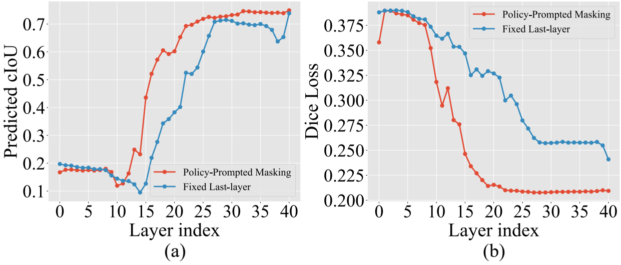

Figure 2: (a) shows that the dynamic layer selection strategy outperforms the fixed last hidden layer strategy across all middle layers. (b) plots the loss of similarity maps against the soft ground-truth mask, demonstrating faster convergence at intermediate layers.

Dynamic layer selection provides insight into the behavior of intermediate layers. By allowing these layers to directly participate in interactions and joint training with SAM—akin to “cheating” in a phone game—each layer’s performance is improved, ultimately resulting in an overall enhancement.

Why Similarity as Mask. To investigate whether the similarity map can serve as a prompt, we conduct two analyses. First, to measure the consistency ($\mathcal{M}_{\text{IoU}}$) between the similarity map and the ground-truth mask, we compute the grid search-based Intersection over Union (IoU) following READ (Qian et al., 2025). Second, to probe whether SAM can understand the semantics encoded in the similarity map, we directly use the similarity map as a logit mask to prompt the original SAM (Kirillov et al., 2023) (without any additional training), denoted by $\mathcal{M}_{\text{prompt}}$. Table 2 shows that SAM can potentially leverage the similarity map as a prompt (17.0% vs. 48.4%). Further, when the similarity map is directly converted into a binary mask for prediction, its performance measured by $\mathcal{M}_{\text{IoU}}$ can even rival that of the trained <SEG>$_{\text{prompt}}$, as evidenced by a 4.3% higher cIoU on the ReasonSeg *test* set (35.0% vs. 30.7%) in the 3rd row.

Table 2: Quantitative analysis of the similarity maps on the ReasonSeg *test* split. $\mathcal{M}_{\text{prompt}}$ indicates mask as a prompt for the original SAM, while $\mathcal{M}_{\text{IoU}}$ quantifies the overlap between the similarity map and the ground-truth mask. <SEG>$_{\text{prompt}}$ refers to <SEG> token as prompt for SAM.

Method	$\mathcal{M}_{\text{prompt}}$		$\mathcal{M}_{\text{IoU}}$		<SEG>$_{\text{prompt}}$	
	gIoU	cIoU	gIoU	cIoU	gIoU	cIoU
LISA-7B (Lai et al., 2024)	**16.1**	**17.0**	32.2	35.6	**47.3**	**48.4**
GSVA-7B (Xia et al., 2024)	15.0	14.7	**33.2**	**37.4**	42.8	43.8
SESAME-7B (Wu et al., 2024)	15.6	15.6	31.6	35.0	34.9	30.7

Summary. Analysis of the similarity maps reveals the following: (a) Similarity maps in LMMs are highly consistent with the ground-truth mask, suggesting that they can potentially serve as prompts for generating the segmentation mask. (b) Dynamic layer selection allows the intermediate layers to directly interact with SAM, resulting in a more discriminative representation, as reflected by the activated regions in the similarity maps. Motivated by the insights from the similarity maps, we leverage it in three ways: as a logit mask to prompt SAM (prompt), as a loss constraint to guide the model on where to “attend” (constraint), and as a policy reward for dynamic layer selection (signal) (see Appendix B.4 for further analysis).

4 Proposed UGround

In this section, we present UGround, which dynamically selects intermediate layers across unrolled transformers and connects them to SAM in a skip-connection fashion, where the similarity map serves as a prompt, thereby contributing to a unified visual grounding paradigm. As depicted in Fig. 3, central to UGround is Policy-Prompted Masking (PPM), consisting of two components: Stochastic Skip Connection (SSC) and Mask as Prompt (MasP). SSC is a reinforcement learning policy that stochastically allows each <SEG> token to slide across unrolled transformer layers, dynamically selecting where it connects to the vision model (*e.g.*, SAM) via a skip connection. MasP, given the selected layer, leverages the similarity map between the <SEG> token and image tokens as a soft logit mask to prompt SAM, providing explicit spatial cues through its activation regions. As the key novelty of our work is PPM, we present it first in Sec. 4.1, then the training objectives in Sec. 4.2.

4.1 Policy-Prompted Masking

Stochastic Skip Connection. Prior works (Lai et al., 2024; Wu et al., 2024; Xia et al., 2024; Rasheed et al., 2024; Ren et al., 2024; Qian et al., 2025) empirically use the embedding from the fixed last hidden layer ($\ell = L$) as the <SEG> token representation $\boldsymbol{h}_{seg}$. In contrast, we exploit intermediate layers ($\ell \in \{1, \ldots, L-1\}$) to derive more discriminative semantics in a skip-connection fashion. To this end, we formulate the problem of selecting a layer for the <SEG> token as a reinforcement learning task. Each layer selection is treated as an action $a \equiv \ell^*$ taken in the state $s \equiv \boldsymbol{h}_{t^*}$, which corresponds to the unrolled <SEG> embeddings across layers. The agent receives a reward r that reflects the consistency of the similarity map with the ground-truth mask. Specifically, let $\mathcal{H}_{t^*}$ represent the hidden states of the <SEG> token from all layers ($\ell \in \{1, \ldots, L\}$) at position t^* of the input sequence $\mathbf{x}$ as $\mathcal{H}_{t^*} = \{\boldsymbol{h}_{t^*}^{(1)}, \boldsymbol{h}_{t^*}^{(2)}, \ldots, \boldsymbol{h}_{t^*}^{(L)}\} \in \mathbb{R}^{L \times d}$, Let $\mathbf{w} \in \mathbb{R}^{L \times d}$ denote learnable weights. The policy distribution $\pi_\theta(\cdot \mid \mathcal{H}_{t^*})$ is defined as

$$\pi_\theta(\ell \mid \mathcal{H}_{t^*}) = \frac{\exp(s_\ell)}{\sum_{j=1}^{L} \exp(s_j)}, s_\ell = \boldsymbol{h}_{t^*}^{(\ell)} \cdot \mathbf{w}_\ell, \tag{4}$$

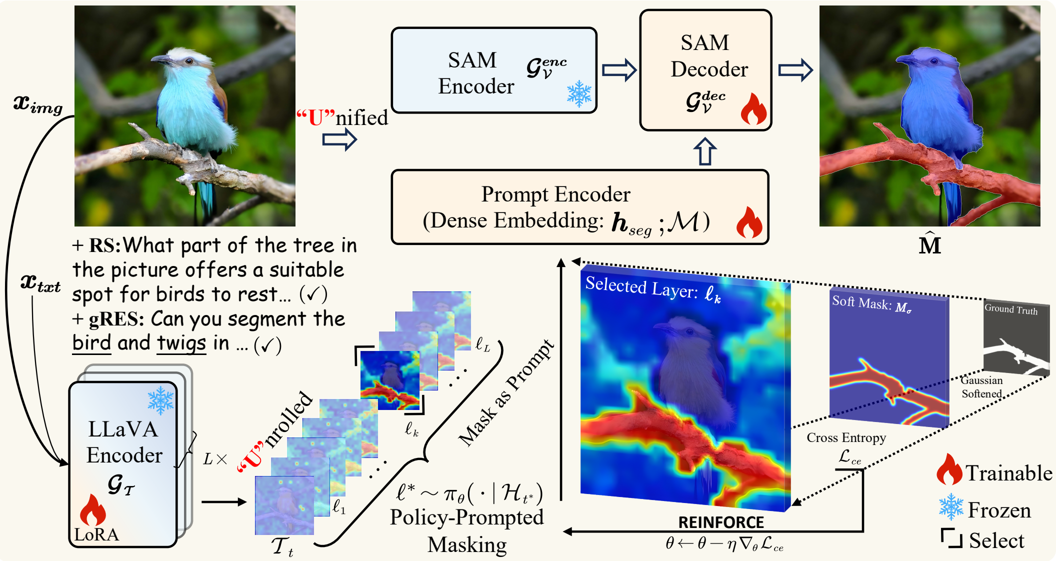
$\boldsymbol{x}_{img}$
$\boldsymbol{x}_{txt}$
"U"nified
SAM Encoder $\mathcal{G}_{\mathcal{V}}^{enc}$
SAM Decoder $\mathcal{G}_{\mathcal{V}}^{dec}$
Prompt Encoder (Dense Embedding: $\boldsymbol{h}_{seg}$;$\mathcal{M}$)
$\hat{\mathbf{M}}$
+ RS: What part of the tree in the picture offers a suitable spot for birds to rest… (✓)
+ gRES: Can you segment the bird and twigs in … (✓)
LLaVA Encoder $\mathcal{G}_{\mathcal{T}}$
LoRA
$L\times$
"U"nrolled
$\mathcal{T}_t$
ℓ_1
ℓ_k
ℓ_L
Mask as Prompt
$\ell^* \sim \pi_\theta(\cdot \mid \mathcal{H}_{t^*})$
Policy-Prompted Masking
Selected Layer: ℓ_k
Soft Mask: M_σ
Ground Truth
Gaussian Softened
Cross Entropy
$\mathcal{L}_{ce}$
REINFORCE
$\theta \leftarrow \theta - \eta \nabla_\theta \mathcal{L}_{ce}$
Trainable
Frozen
Select

Figure 3: Overview of our proposed UGround. Central to UGround is Policy-Prompted Masking (PPM), which stochastically selects layer ℓ^* among "Unrolled" transformers from a policy distribution $\pi_\theta(\cdot \mid \mathcal{H}_{t^*})$ at which it connects to the vision model (*e.g.*, SAM) in a skip-connection fashion. Given the layer ℓ^*, MasP uses the similarity map as a soft logit mask to prompt SAM for mask generation, wherein we advance visual grounding within a "Unified" paradigm from an attribute perspective.

where s_ℓ is the logit scores for each layer. $\boldsymbol{h}_{t^*}^{(\ell)}$ is the `<SEG>` embedding at layer ℓ and $\mathbf{w}_\ell$ is the corresponding learnable weight. The agent chooses a layer ℓ according to a categorical distribution parameterized by learnable weights $\mathbf{w}$. During training, the layer ℓ^* is sampled from this distribution to allow exploration as $\ell^* \sim \pi_\theta(\cdot \mid \mathcal{H}_{t^*})$, To reduce variance, we introduce a baseline b, which can be an EMA-smoothed reward or a critic network prediction. The actual reward r is derived from the similarity map, as described in Algorithm (1) steps 5-8. We therefore formulate the REINFORCE gradient as

$$\nabla_\theta J(\theta) = \mathbb{E}_{\ell^* \sim \pi_\theta(\cdot \mid \mathcal{H}_{t^*})} \Big[(r - b)\, \nabla_\theta \log \pi_\theta(\ell^* \mid \mathcal{H}_{t^*}) \Big], \tag{5}$$

where the log-probability of the sampled action $a \equiv \ell^*$ is weighted by the advantage $r - b$. To get the reward r, we first compute the similarity map $\mathcal{M}$ between the `<SEG>` token and image tokens at layer ℓ and its corresponding soft mask $\mathcal{M}_\sigma$. Consider a sequence of discrete image tokens $\mathbf{z} = (z_1, z_2, \ldots, z_k)$ in the input sequence $\mathbf{x}$, where k is the number of image tokens. The image token embeddings across layers are then denoted as $\mathcal{H}_{\mathbf{z}} = \{\boldsymbol{h}_z^{(\ell)} \mid z \in \mathbf{z},\ \ell = 1, \ldots, L\} \in \mathbb{R}^{k \times L \times d}$, where $\boldsymbol{h}_z^{(\ell)}$ is the embedding of the z-th image token at layer ℓ. Given the `<SEG>` token embedding $\boldsymbol{h}_{t^*}^{(\ell)} \in \mathbb{R}^d$ and the image token embeddings $\mathcal{H}_{\mathbf{z}}^{(\ell)} \in \mathbb{R}^{k \times d}$ at the selected layer ℓ, the similarity scores can be computed as

$$\mathcal{S}^{(\ell)} = \mathcal{H}_{\mathbf{z}}^{(\ell)}\, {h_{t^*}^{(\ell)}}^\top \in \mathbb{R}^k, \tag{6}$$

where each element $\mathcal{S}_i^{(\ell)} = (h_{z_i}^{(\ell)})^\top h_{t^*}^{(\ell)}$ represents the similarity between the `<SEG>` token and the i-th selected image token at layer ℓ. $\mathcal{S}^{(\ell)}$ are arranged in a 2D grid, and interpolated to obtain the soft logit mask $\mathcal{M} \in [0,1]^{H \times W}$. Let the ground-truth mask be $M \in \{0,1\}^{H \times W}$, which we regard as a function $M : \{1, \ldots, H\} \times \{1, \ldots, W\} \to \{0,1\}$ over the discrete pixel grid. We extend M to the continuous domain $\mathbb{R}^2$ by assigning each pixel a constant value on its corresponding region in the plane. Applying Gaussian smoothing to this extended function yields a continuous-valued function $M_\sigma : \mathbb{R}^2 \to [0,1]$, where M_σ serves as the soft label (heatmap). Formally, M_σ can be expressed as a convolution integral as $M_\sigma(u,v) = \iint_{\mathbb{R}^2} M(x,y)\, G_\sigma(u-x, v-y)\, dx\, dy$, where $G_\sigma(x,y) \propto \exp(-\frac{x^2+y^2}{2\sigma^2})$, is a 2D Gaussian kernel with standard deviation σ. The reward for REINFORCE is computed using the similarity map $\mathcal{M}$ and the soft label M_σ as $r = -\big(\mathcal{L}_{bce}(\mathcal{M}, M_\sigma) + \mathcal{L}_{dice}(\mathcal{M}, M_\sigma)\big)$, where $\mathcal{L}_{bce}$ and $\mathcal{L}_{dice}$ denote the Gaussian BCE and Dice losses defined over the similarity map $\mathcal{M}$. The policy loss is then defined as

$$\mathcal{L}_{\text{policy}} = -(r - b_t)\, \log \pi_\theta(\ell^* \mid \mathcal{H}_{t^*}). \tag{7}$$

Algorithm 1 Policy-Prompted Masking Algorithm

```
Require:
    Given unrolled transformer layers with $L$ layers, $\mathcal{H}_{t^*} \in \mathbb{R}^{L\times d}$ is hidden states of <SEG> token, $\mathcal{H}_{\mathbf{z}} \in \mathbb{R}^{k\times L\times d}$ is hidden states of image tokens; $\mathbf{w}$ is learnable weights $\mathbf{w} \in \mathbb{R}^{L\times d}$;
    $M_\sigma : \mathbb{R}^2 \to [0,1]$, where $M_\sigma$ is the soft heatmap, with a Gaussian kernel $G_\sigma(x,y)$; $r$ is the reward score, $b$ is the baseline, $M \in \{0,1\}^{H\times W}$ is ground-truth mask;
    $\mathcal{T}$ denotes the number of forward passes, each of which corresponds to an independent policy sampling followed by a mask prediction.
Ensure:
    Selected layer $\ell_t^*$ and similarity map $\mathcal{M}_t$
for $t = 1, \dots, \mathcal{T}$ do
    $s_\ell = \boldsymbol{h}_{t^*}^{(\ell)} \cdot \mathbf{w}_\ell$ for $\ell = 1, \dots, L$
    $\pi_\theta(\ell \mid \mathcal{H}_{t^*}) = \frac{\exp(s_\ell)}{\sum_{j=1}^{L}\exp(s_j)}$
    $\ell^* \sim \pi_\theta(\cdot \mid \mathcal{H}_{t^*})$
    $\mathcal{S}^{(\ell^*)} = \mathcal{H}_{\mathbf{z}}^{(\ell^*)}\, {h_{t^*}^{(\ell^*)}}^\top \in \mathbb{R}^k$
    $\mathcal{M} \in [0,1]^{H\times W} \leftarrow \mathcal{S}^{(\ell^*)}$
    $M_\sigma(u,v) = \iint_{\mathbb{R}^2} M(x,y)\, G_\sigma(u-x, v-y)\, dx\, dy$
    $r = -\big(\mathcal{L}_{bce}(\mathcal{M}, M_\sigma) + \mathcal{L}_{dice}(\mathcal{M}, M_\sigma)\big)$
    $b_t = \alpha b_{t-1} + (1-\alpha) r$
    $\mathcal{L}_{\text{policy}} = -(r - b_t)\log \pi_\theta(\ell^* \mid \mathcal{H}_{t^*})$
    $\theta \leftarrow \theta - \eta \nabla_\theta \mathcal{L}_{\text{policy}}$
end for
return $\{\ell_t^*, \mathcal{M}_t\}_{t=1}^{\mathcal{T}}$
```

Algorithm (1) outlines a single forward pass of the PPM. The transformer layers are stacked sequentially. By skipping the subsequent $L - \ell^*$ layers, the PPM allows layer ℓ^* to connect directly to SAM in a skip-connection manner, thereby mitigating cumulative errors that arise from layer-by-layer propagation through intermediate correction (*i.e.*, a shortcut that bypasses subsequent layers). Across multiple forward passes (from 1 to $\mathcal{T}$), the PPM dynamically alters the model's internal connectivity, analogous to the dropout mechanism: although all layers are virtually connected to SAM, only one path is activated per pass. This stochastic sampling can be interpreted as a form of Monte Carlo uncertainty estimation (Gal & Ghahramani, 2016), which quantifies predictive uncertainty via multiple stochastic forward passes. In the context of PPM, each forward pass activates a different layer-path to SAM, and the ensemble of these paths (*i.e.*, 32 in LLaVA) alleviates over-reliance on any single trajectory, enhancing the model's robustness.

Mask as Prompt. Compared with <SEG> tokens, the similarity map provides more explicit spatial cues, as analyzed in Sec. 3.2. We use the similarity map as a logit mask to prompt SAM. Accordingly, we reformulate Eq. (3) as $\hat{\mathbf{M}} = \mathcal{G}_{\mathcal{V}}^{dec}(\mathbf{f}, \boldsymbol{h}_{seg}, \mathcal{M})$. The similarity map is continuously differentiable, allowing its gradients to be backpropagated through the SAM module for implicit optimization. To further guide the model to focus on target regions, we supervise the similarity map $\mathcal{M}$ by imposing a constraint (*e.g.*, using BEC or Dice loss) against a soft ground-truth mask M_σ, providing explicit guidance on where the model should "attend".

4.2 Training Objectives

Apart from the text generation loss $\mathcal{L}_{txt}$ in $\mathcal{G}_{\mathcal{T}}$, and the segmentation mask loss $\mathcal{L}_{mask}$ in $\mathcal{G}_{\mathcal{V}}^{dec}$ (Lai et al., 2024; Wu et al., 2024), we use policy loss $\mathcal{L}_{\text{policy}}$ for stochastic skip connection, and binary cross-entropy (BCE) loss and Dice loss for similarity map as

$$\begin{aligned}\mathcal{L}_{\text{policy}} &= -(r - b_t)\,\log \pi_\theta(\ell^* \mid \mathcal{H}_{t^*}),\\ \mathcal{L}_{\mathcal{M}} &= \lambda_{bce}\mathcal{L}_{bce}(\mathcal{M}, M_\sigma) + \lambda_{dice}\mathcal{L}_{dice}(\mathcal{M}, M_\sigma),\end{aligned} \tag{8}$$

where M_σ is the soft ground-truth target, λ denotes the loss weight, $\mathcal{M}$ is the similarity map. The overall objective $\mathcal{L}$ summarizes those losses in Eq. (8), weighted by λ_{txt}, λ_{mask}, $\lambda_{\mathcal{M}}$, and λ_{policy} as

$$\mathcal{L} = \lambda_{txt}\mathcal{L}_{txt} + \lambda_{mask}\mathcal{L}_{mask} + \lambda_{\mathcal{M}}\mathcal{L}_{\mathcal{M}} + \lambda_{policy}\mathcal{L}_{\text{policy}}. \tag{9}$$

5 Experiment

5.1 Experimental Setting

Implementation Details. We observe that the center scaling and cropping operation in CLIP may crop out target objects. To address this issue and to align the similarity map with SAM's input, we adopt SAM's transformation strategy, scaling the longer side of the image to 336 and padding the image for the CLIP input 336×336. For results on ReasonSeg, UGround-7B-LLaVA1.5 is trained on 1 NVIDIA A100 GPU 80GB for about 2 days, UGround-13B-LLaVA1.5 for about 13 hours. The training relies solely on ReasonSeg and a referring segmentation dataset (∼10k images). We use LoRA (Hu et al., 2022) for efficient fine-tuning, using $lora\_r = 8$ for 7B and 64 for 13B. We use the AdamW (Loshchilov & Hutter, 2019) optimizer with an initial learning rate of 3e-4, scheduled by WarmupDecayLR with 100 warmup steps. Loss weights are set as $\lambda_{mask} = \lambda_{txt} = 1.0$, $\lambda_{policy} = 0.1$, $\lambda_{bce} = 2.0$, and $\lambda_{dice} = 4.0$.

Table 3: Benchmarking reasoning segmentation models on the ReasonSeg dataset, sorted in ascending order of cIoU on the test set. *: reproduced from official models. ft: fine-tuned on 239 samples.

Method	val		test					
	overall		short query		long query		overall	
	gIoU	cIoU	gIoU	cIoU	gIoU	cIoU	gIoU	cIoU
X-Decoder (Zou et al., 2023a)	22.6	17.9	20.4	11.6	22.2	17.5	21.7	16.3
Grounded-SAM (Liu et al., 2024b)	26.0	14.5	17.8	10.8	22.4	18.6	21.3	16.4
SEEM (Zou et al., 2024)	25.5	21.2	20.1	11.5	25.6	20.8	24.3	18.7
OVSeg (Liang et al., 2023)	28.5	18.6	18.0	15.5	28.7	22.5	26.1	20.8
GRES (Liu et al., 2023)	22.4	19.9	17.6	15.0	22.6	23.8	21.3	22.0
*SESAME (Wu et al., 2024)	40.3	41.6	28.9	26.3	37.3	31.9	34.9	30.7
LLaVA1.5-7B + OVSeg (Lai et al., 2024)	38.2	23.5	24.2	18.7	44.6	37.1	39.7	31.8
*GSVA (Xia et al., 2024)	45.6	41.5	37.9	36.5	44.3	46.0	42.8	43.8
*PixelLM (Ren et al., 2024)	49.7	49.6	39.5	38.8	49.5	45.6	47.1	44.3
LISA-7B (Lai et al., 2024)	52.9	54.0	40.6	40.6	49.4	51.0	47.3	48.4
HyperSeg-3B (Wei et al., 2025)	59.2	56.7	-	-	-	-	-	-
VISA-7B (Yan et al., 2024)	52.7	57.8	-	-	-	-	-	-
VideoLISA-3.8B (Bai et al., 2024)	61.4	67.1	43.8	42.7	56.9	57.7	53.8	54.4
LISA-7B-LLaVA1.5 (ft) (Lai et al., 2024)	61.3	62.9	48.3	46.3	57.9	59.7	55.6	56.9
READ-7B-LLaVA1.5 (ft) (Qian et al., 2025)	59.8	67.6	52.6	49.5	60.4	61.0	58.5	58.6
LISA++-7B-LLaVA1.5 (ft) (Yang et al., 2023)	64.2	68.1	49.6	**51.1**	59.3	61.7	57.0	59.5
RSVP-GPT (Lu et al., 2025)	64.7	63.1	**55.4**	50.4	61.9	62.5	60.3	60.0
UGround-7B-LLaVA1.5 (ft)	**66.1**	**72.1**	55.1	48.5	**66.3**	**70.2**	**63.6**	**65.4**
LLaVA1.5-13B + OVSeg (Lai et al., 2024)	37.9	26.4	27.1	19.4	46.1	40.6	41.5	34.1
LISA-13B-LLaVA1.5 (Lai et al., 2024)	57.7	60.3	50.8	50.0	54.7	50.9	53.8	50.8
LISA-13B-LLaVA1.5(ft) (Lai et al., 2024)	65.0	72.9	55.4	50.6	63.2	65.3	61.3	62.2
READ-13B-LLaVA1.5 (ft) (Qian et al., 2025)	-	-	55.4	**53.7**	64.4	65.1	62.2	62.8
UGround-13B-LLaVA1.5 (ft)	**67.9**	**74.9**	**57.2**	50.9	**67.5**	**69.4**	**65.0**	**65.5**

Table 4: Benchmarking referring segmentation models on the RefCOCO(+/g) dataset, sorted in ascending order of cIoU on the RefCOCOg val set.

Method	refCOCO			refCOCO+			refCOCOg	
	val	testA	testB	val	testA	testB	val(U)	test(U)
MCN (Luo et al., 2020)	62.4	64.2	59.7	50.6	55.0	44.7	49.2	49.4
VLT (Ding et al., 2021)	67.5	70.5	65.2	56.3	61.0	50.1	55.0	57.7
CRIS (Wang et al., 2022)	70.5	73.2	66.1	62.3	68.1	53.7	59.9	60.4
LAVT (Yang et al., 2022)	72.7	75.8	68.8	62.1	68.4	55.1	61.2	62.1
X-Decoder (Zou et al., 2023a)	-	-	-	-	-	-	64.6	-
ReLA (Liu et al., 2023)	73.8	76.5	70.2	66.0	71.0	57.7	65.0	66.0
SEEM (Zou et al., 2024)	-	-	-	-	-	-	65.7	-
MagNet (Chng et al., 2024)	76.6	78.3	72.2	68.1	73.6	68.1	67.8	69.3
Segment Anyword (Liu et al., 2025)	55.3	47.9	66.0	55.6	47.4	67.0	58.4	60.1
VISA-7B (Yan et al., 2024)	72.4	75.5	68.1	59.8	64.8	53.1	65.5	66.4
SESAME (Wu et al., 2024)	74.7	-	-	64.9	-	-	66.1	-
LISA-7B (Lai et al., 2024)	74.9	79.1	72.3	65.1	70.8	58.1	67.9	70.6
CoRes (Bao et al., 2024)	76.0	78.6	72.5	65.1	70.0	58.6	69.0	70.7
PixelLM-7B (Ren et al., 2024)	73.0	76.5	68.2	66.3	71.7	58.3	69.3	70.5
READ-7B (Qian et al., 2025)	78.1	80.2	73.2	68.4	73.7	60.4	70.1	71.4
SegLLM-7B (Wang et al., 2025)	80.2	81.5	75.4	70.3	73.0	62.5	72.6	73.6
GSVA-7B (Xia et al., 2024)	77.2	78.9	73.5	65.9	69.6	59.8	72.7	73.3
OMG-LLaVA (Zhang et al., 2024b)	78.0	80.3	74.1	69.1	73.1	63.0	72.9	72.9
GLaMM-7B (Rasheed et al., 2024)	79.5	83.2	76.9	72.6	**78.7**	64.6	74.2	74.9
POPEN-7B (Zhu et al., 2025)	79.3	82.0	74.1	**73.1**	77.0	65.1	**75.4**	75.6
UGround-7B	**80.6**	**83.5**	**77.7**	72.8	77.5	**65.6**	74.7	**76.1**

Table 5: Benchmarking generalized referring expression segmentation (GRES) models on the gRefCOCO (Liu et al., 2023) dataset, sorted in ascending order of cIoU on the gRefCOCO validation set. Values are taken from (Liu et al., 2023). N-acc.: the accuracy of correct null-target classification. ft: fine-tuned on gRefCOCO training set.

Method	Validation Set			Test Set A			Test Set B		
	gIoU	cIoU	N-acc.	gIoU	cIoU	N-acc.	gIoU	cIoU	N-acc.
MattNet (Yu et al., 2018)	48.24	47.51	41.15	59.30	58.66	44.04	46.14	45.33	41.32
LTS (Jing et al., 2021)	52.70	52.30	-	62.64	61.87	-	50.42	49.96	-
VLT (Ding et al., 2021)	52.00	52.51	47.17	63.20	62.19	48.74	50.88	50.52	47.82
CRIS (Wang et al., 2022)	56.27	55.34	-	63.42	63.82	-	51.79	51.04	-
LAVT (Yang et al., 2022)	58.40	57.64	49.32	65.90	65.32	49.25	55.83	55.04	48.46
ReLA (Liu et al., 2023)	63.60	62.42	56.37	70.03	69.26	59.02	61.02	59.88	58.40
LISA-Vicuna-7B (Lai et al., 2024)	32.21	38.72	2.71	48.54	52.55	6.37	39.65	44.79	5.00
GSVA-Vicuna-7B (Xia et al., 2024)	63.32	61.70	56.45	70.11	69.23	63.50	61.34	60.26	58.42
LISA-Vicuna-7B (ft) (Lai et al., 2024)	61.63	61.76	54.67	66.27	68.50	50.01	58.84	60.63	51.91
GSVA-Vicuna-7B (ft) (Xia et al., 2024)	66.47	63.29	62.43	71.08	69.93	65.31	62.23	60.47	60.56
UGround-LLaVA1.5-7B(ft)	**72.46**	**65.56**	**74.53**	**74.29**	**70.87**	**73.93**	**66.85**	**61.84**	**71.22**

5.2 Comparison with the State-of-the-Art

Results on ReasonSeg Dataset. In Table 3, UGround achieves competitive performance compared with the recent state-of-the-art RSVP-GPT. On the ReasonSeg validation set, UGround-7B improves over RSVP-GPT by +1.4% gIoU and +9.0% cIoU. On the test set, UGround surpasses RSVP-GPT by +3.3% gIoU and +5.4% cIoU. At the larger scale, UGround-13B further pushes the state of the art, outperforms READ-13B by up to +2.8% gIoU and +2.7% cIoU. These results validate UGround's effectiveness in complex reasoning-oriented segmentation.

Results on RefCOCO(+/g) Dataset. In Table 4, UGround-7B achieves overall stronger performance compared with the recent state-of-the-art POPEN-7B. On RefCOCO, UGround surpasses POPEN-7B by +1.3% (val), +1.5% (testA), and +3.6% (testB), establishing clear new records across all splits. On the RefCOCOg dataset, UGround standout on test with a score of 76.1%, marking a +0.5% improvement over POPEN-7B. These results highlight that UGround consistently outperforms POPEN-7B on most benchmarks.

Results on gRefCOCO Dataset. In Table 5, UGround-7B achieves substantially stronger performance compared with the recent state-of-the-art GSVA-7B (ft) on the gRefCOCO dataset. On the validation set, UGround improvies over GSVA-7B (ft) by +5.99% gIoU, +2.27% cIoU, and +12.10% N-acc, respectively. On Test A, UGround surpasses GSVA-7B (ft) by +3.21% gIoU, +0.94% cIoU, and +8.62% N-acc. These results demonstrate that UGround not only reflects its strength in multi-object segmentation but also excels in correctly identifying empty targets (N-acc).

5.3 Ablation Study

In this section, we conduct an ablation study to analyze the contribution of each component. We report the gIoU and cIoU performance on the *val* set of ReasonSeg dataset.

Effect of the components of PPM. In Table 6, comparing Exp. 3, Exp. 6, we observe that dynamic layer selection yields a clear improvement (+2.07% gIoU and +5.02% cIoU), highlighting the benefit of leveraging information across multiple layers. Moreover, the decomposition indicates that using the similarity map as a prompt ($\mathcal{M}_{\text{prompt}}$) contributes the most (e.g., Exp. 1 vs. Exp. 2, and Exp. 4 vs. Exp. 5) within this paradigm.

Table 6: Ablation study on PPM.

Exp. ID	SSC	<SEG>$_{\text{prompt}}$	$\mathcal{M}_{\text{prompt}}$	gIoU	cIoU
1		✓		19.13	15.62
2			✓	60.30	53.86
3		✓	✓	64.06	67.05
4	✓	✓		31.76	34.08
5	✓		✓	52.14	52.42
6	✓	✓	✓	**66.13**	**72.07**

Effect of explicit constraints for similarity map $\mathcal{M}$. In Table 7, Exp. 1, 2, and 5 optimize the similarity map against hard labels (binary masks), while Exp. 3, 4, and 6 optimize it against soft labels (continuous masks). The results demonstrate that converting the ground-truth mask into a Gaussian heatmap smooths the object boundaries, leading to performance gains of +2.21% gIoU and +3.52% cIoU when comparing Exp. 5 and Exp. 6.

Table 7: Ablation study on explicit constraints for similarity map $\mathcal{M}$.

Exp. ID	BCE	DICE	Gaussian BCE	Gaussian DICE	gIoU	cIoU
1	✓				64.56	71.44
2		✓			64.57	68.63
3			✓		63.16	65.74
4				✓	65.80	**73.49**
5	✓	✓			63.92	68.55
6			✓	✓	**66.13**	72.07

Effect of policy reward components. We use the negative loss of the similarity map relative to the ground-truth mask as the reward. During training, it is treated as a scalar and detached from the computation graph. In Table 8, comparing Exp. 1 and Exp. 2, we observe that using r_{bce} as the reward signal outperforms using r_{dice}, yielding a gain of +2.03% gIoU and +1.20% cIoU.

Table 8: Ablation study on reward.

Exp. ID	r_{bce}	r_{dice}	gIoU	cIoU
1	✓		65.37	69.53
2		✓	63.34	68.33
3	✓	✓	**66.13**	**72.07**

6 Analysis

Complexity Analysis. To justify the complexity of RL-based layer selection (RL-gating), we compare it against a simpler non-RL alternative—soft-gating, *i.e.*, a learned soft-attention mechanism that produces a weighted average over layer outputs. We report results on ReasonSeg val set. In Table 9, RL-gating consistently outperforms soft-gating, with gains of +4.94% in gIoU and +6.55% in cIoU.

Table 9: RL-gating vs. soft-gating.

Exp. ID	Method	gIoU	cIoU
1	soft-gating	61.19	65.52
2	RL-gating	66.13	72.07

Table 10: Comparing the training cost of our UGround to state-of-the-art methods.

Model	Training Latency (s)	Memory Usage (GB)	Trainable (%)	Trainable Params	Total Params
SESAME (Wu et al., 2024)	1.11	23.15	3.73%	288.25M	7.73B
PixelLM (Ren et al., 2024)	1.22	23.02	5.25%	375.72M	7.16B
LISA (Lai et al., 2024)	1.26	23.68	3.74%	288.25M	7.71B
GSVA (Xia et al., 2024)	2.13	25.73	3.73%	288.26M	7.73B
UGround	2.97	28.16	3.72%	288.40M	7.75B

Table 11: Comparing the runtime speed of our UGround to state-of-the-art methods.

Model	GSVA (Xia et al., 2024)	SESAME (Wu et al., 2024)	LISA (Lai et al., 2024)	PixelLM (Ren et al., 2024)	UGround
Speed (FPS)	3.98	4.64	4.68	9.24	4.12

Table 12: Comparison on MUSE benchmark. Numbers are cited from PixelLM (Ren et al., 2024).

Method	w/o SAM	Val		Test					
		overall		few targets		many targets		overall	
		gIoU	cIoU	gIoU	cIoU	gIoU	cIoU	gIoU	cIoU
SEEM (Zou et al., 2023b)	✓	13.6	16.2	23.6	24.9	8.5	13.2	11.7	15.7
LISA-7B (Lai et al., 2024)	✗	18.8	29.0	24.7	36.5	9.6	24.5	12.8	27.1
LISA-7B$_{\text{rec}}$ (Lai et al., 2024)	✗	24.5	31.1	30.0	30.9	12.4	23.2	16.2	24.8
LISA-7B$_{\text{aug}}$ (Lai et al., 2024)	✗	42.0	46.1	43.5	52.0	37.7	42.3	38.9	44.4
PixelLM-7B (Ren et al., 2024)	✓	42.6	50.7	44.6	59.2	37.7	42.8	39.2	46.3
UGround-7B	✓	**52.4**	**56.4**	**46.2**	**69.7**	**38.8**	**46.9**	**40.1**	**50.4**

Table 13: Comparisons of the state-of-the-art "see" and "segment" results on augmented FP-refcoco(+/g) *val* set. "FP"(False Premise) denotes a query for an object absent from the image.

Method	FP-RefCOCO		FP-RefCOCO+		FP-RefCOCOg	
	See	Segment	See	Segment	See	Segment
LISA-7B (Lai et al., 2024)	51.36	44.00	51.32	39.62	51.25	39.64
Cascading (Wu et al., 2024)	75.59	55.18	75.03	48.64	76.07	49.98
SESAME (Wu et al., 2024)	79.84	57.93	80.00	50.81	81.78	53.79
READ (Qian et al., 2025)	82.87	61.50	83.51	54.54	84.67	56.12
UGround	**85.86**	**62.80**	**85.10**	**56.03**	**86.86**	**58.55**

Runtime Analysis. To assess the computational costs of UGround, we report training and inference latency on a single NVIDIA A100-SXM4-40GB GPU in Table 10 and Table 11. We train on the ReasonSeg train split over 400 samples for 1 epoch (200 steps), with a batch size of 2. Training Latency (s) refers to the average time per iteration during the 200-step training process (including forward, backward, and optimizer step), and Memory Usage refers to the MaxMemAllocated observed within the 200 steps. We also report the model's Trainable Percentage (Trainable Parameters / Total Parameters). For inference, we evaluate on the ReasonSeg test split over 799 samples, with a batch size of 1. Speed (FPS) refers to the average frames per second computed over the 799 samples. In Table 10, UGround exhibits a higher training latency (2.97s) than LISA (Lai et al., 2024)(1.26s) due to the explicit optimization of the similarity map during the backward pass. In Table 10, UGround achieves a comparable inference runtime to LISA (Lai et al., 2024) and SESAME (Wu et al., 2024).

Generalization Analysis. To demonstrate broader generalization of UGround, we report results on MUSE benchmark. MUSE aims for multi-target reasoning segmentation (Ren et al., 2024). In Table 12, UGround-7B consistently outperforms PixelLM-7B across all splits of the MUSE benchmark. It improves the Val overall cIoU by +5.7% and boosts the challenging "few-targets" cIoU by +10.5%. On the Test overall set, UGround also achieves a +4.1% cIoU gain, yielding a clear performance margin over PixelLM-7B. Also, we report results on augmented FP-refcoco(+/g) under false premises. In Table 13, UGround outperforms READ across all FP-refcoco(+/g) splits, with gains of +1.59% to +2.99% in "see" accuracy and +1.30% to +2.43% in segment scores (cIoU).

7 Conclusion

In this work, we first visualize all unrolled Transformer layers of LMMs, represented by LLaVA, and analyze the influence of intermediate layers on downstream task decoding. Building on this analysis, we present UGround, which features a dynamic layer selection and prompting mechanism—Policy-Prompted Masking (PPM). PPM enables intermediate layers to connect to the SAM decoder in a skip-connection-like manner and adjust its connectivity in a dropout-like fashion under the "mask as prompt" paradigm, together contributing to unified visual grounding. Our future work aims to further investigate how the <SEG> token interacts with the integrated SAM module for alignment.

References

Jean-Baptiste Alayrac, Jeff Donahue, Pauline Luc, Antoine Miech, Iain Barr, Yana Hasson, Karel Lenc, Arthur Mensch, Katherine Millican, Malcolm Reynolds, et al. Flamingo: a visual language model for few-shot learning. In NeurIPS, 2022.

Vijay Badrinarayanan, Alex Kendall, and Roberto Cipolla. Segnet: A deep convolutional encoder-decoder architecture for image segmentation. In TPAMI, 2017.

Zechen Bai, Tong He, Haiyang Mei, Pichao Wang, Ziteng Gao, Joya Chen, Zheng Zhang, and Mike Zheng Shou. One token to seg them all: Language instructed reasoning segmentation in videos. In NeurIPS, 2024.

Xiaoyi Bao, Siyang Sun, et al. CoRes: Orchestrating the dance of reasoning and segmentation. In ECCV, 2024.

Nicolas Carion, Francisco Massa, Gabriel Synnaeve, Nicolas Usunier, Alexander Kirillov, and Sergey Zagoruyko. End-to-end object detection with transformers. In ECCV, 2020.

Bowen Cheng, Ishan Misra, Alexander G Schwing, Alexander Kirillov, and Rohit Girdhar. Masked-attention mask transformer for universal image segmentation. In CVPR, 2022.

Yong Xien Chng, Henry Zheng, Yizeng Han, et al. Mask grounding for referring image segmentation. In CVPR, 2024.

Henghui Ding, Chang Liu, Suchen Wang, and Xudong Jiang. Vision-language transformer and query generation for referring segmentation. In ICCV, 2021.

Yarin Gal and Zoubin Ghahramani. Dropout as a bayesian approximation: Representing model uncertainty in deep learning. In ICML, 2016.

Kaiming He, Georgia Gkioxari, Piotr Dollár, and Ross Girshick. Mask R-CNN. In CVPR, 2017.

Edward J. Hu, Yelong Shen, Phillip Wallis, Zeyuan Allen-Zhu, Yuanzhi Li, Shean Wang, Lu Wang, and Weizhu Chen. LoRA: Low-rank adaptation of large language models. In ICLR, 2022.

Ya Jing, Tao Kong, Wei Wang, Liang Wang, Lei Li, and Tieniu Tan. Locate then segment: A strong pipeline for referring image segmentation. In CVPR, 2021.

Alexander Kirillov, Ross Girshick, Kaiming He, and Piotr Dollár. Panoptic feature pyramid networks. In CVPR, 2019a.

Alexander Kirillov, Kaiming He, Ross Girshick, Carsten Rother, et al. Panoptic segmentation. In CVPR, 2019b.

Alexander Kirillov, Eric Mintun, Nikhila Ravi, Hanzi Mao, Chloe Rolland, Laura Gustafson, Tete Xiao, Spencer Whitehead, Alexander C Berg, et al. Segment anything. In ICCV, 2023.

Xin Lai, Zhuotao Tian, Yukang Chen, Yanwei Li, Yuhui Yuan, Shu Liu, and Jiaya Jia. LISA: Reasoning segmentation via large language model. In CVPR, 2024.

Bo Li, Yuanhan Zhang, Liangyu Chen, Jinghao Wang, Fanyi Pu, Joshua Adrian Cahyono, Jingkang Yang, Chunyuan Li, and Ziwei Liu. Otter: A multi-modal model with in-context instruction tuning. In TPAMI, 2025.

Junnan Li, Dongxu Li, Silvio Savarese, and Steven Hoi. Blip-2: Bootstrapping language-image pre-training with frozen image encoders and large language models. In ICML, 2023.

Xiangtai Li, Haobo Yuan, Wei Li, Henghui Ding, Size Wu, Wenwei Zhang, Yining Li, Kai Chen, and Chen Change Loy. Omg-Seg: Is one model good enough for all segmentation? In CVPR, 2024.

Feng Liang, Bichen Wu, Xiaoliang Dai, Kunpeng Li, Yinan Zhao, Hang Zhang, Peizhao Zhang, Peter Vajda, and Diana Marculescu. Open-vocabulary semantic segmentation with mask-adapted clip. In CVPR, 2023.

Chang Liu, Henghui Ding, and Xudong Jiang. GRES: Generalized referring expression segmentation. In CVPR, 2023.

Haotian Liu, Chunyuan Li, Qingyang Wu, et al. Visual instruction tuning. In NeurIPS, 2024a.

Shilong Liu, Zhaoyang Zeng, Tianhe Ren, Feng Li, Hao Zhang, Jie Yang, Chunyuan Li, Jianwei Yang, and et al Su, Hang. Grounding DINO: Marrying dino with grounded pre-training for open-set object detection. In ECCV, 2024b.

Shu Liu, Lu Qi, and et al. Qin, Haifang. Path aggregation network for instance segmentation. In CVPR, 2018.

Zhihua Liu, Amrutha Saseendran, Lei Tong, Xilin He, Fariba Yousefi, Nikolay Burlutskiy, Dino Oglic, Tom Diethe, Philip Alexander Teare, Huiyu Zhou, et al. Segment anyword: Mask prompt inversion for open-set grounded segmentation. In ICML, 2025.

Jonathan Long and et al. Shelhamer, Evan. Fully convolutional networks for semantic segmentation. In CVPR, 2015.

Ilya Loshchilov and Frank Hutter. Decoupled weight decay regularization. In ICLR, 2019.

Yi Lu, Jiawang Cao, Yongliang Wu, Bozheng Li, Licheng Tang, Yangguang Ji, Chong Wu, Jay Wu, and Wenbo Zhu. RSVP: Reasoning segmentation via visual prompting and multi-modal chain-of-thought. In ACL, 2025.

Gen Luo, Yiyi Zhou, Xiaoshuai Sun, Liujuan Cao, Chenglin Wu, Cheng Deng, and Rongrong Ji. Multi-task collaborative network for joint referring expression comprehension and segmentation. In CVPR, 2020.

Tengchao Lv, Yupan Huang, Jingye Chen, Lei Cui, Shuming Ma, Yaoyao Chang, Shaohan Huang, Wenhui Wang, Li Dong, et al. Kosmos-2.5: A multimodal literate model. In arXiv, 2023.

Junhua Mao, Jonathan Huang, Alexander Toshev, Oana Camburu, and et al. Yuille, Alan L. Generation and comprehension of unambiguous object descriptions. In CVPR, 2016.

Zhiliang Peng, Wenhui Wang, Li Dong, Yaru Hao, Shaohan Huang, Shuming Ma, Qixiang Ye, et al. Grounding multimodal large language models to the world. In ICLR, 2024.

Renjie Pi, Jiahui Gao, Shizhe Diao, Rui Pan, Hanze Dong, Jipeng Zhang, Lewei Yao, Jianhua Han, Hang Xu, Lingpeng Kong, and Tong Zhang. DetGPT: Detect what you need via reasoning. In EMNLP, 2023.

Rui Qian, Xin Yin, and Dejing Dou. Reasoning to attend: Try to understand how <SEG> token works. In CVPR, 2025.

Alec Radford, Jong Wook Kim, Chris Hallacy, Aditya Ramesh, Gabriel Goh, Sandhini Agarwal, Girish Sastry, Amanda Askell, Pamela Mishkin, Jack Clark, et al. Learning transferable visual models from natural language supervision. In ICML, 2021.

Hanoona Rasheed, Muhammad Maaz, Sahal Shaji, Abdelrahman Shaker, Salman Khan, Hisham Cholakkal, Rao M Anwer, Eric Xing, Ming-Hsuan Yang, and Fahad S Khan. GlaMM: Pixel grounding large multimodal model. In CVPR, 2024.

Zhongwei Ren, Zhicheng Huang, Yunchao Wei, Yao Zhao, Dongmei Fu, Jiashi Feng, and Xiaojie Jin. PixelLM: Pixel reasoning with large multimodal model. In CVPR, 2024.

Olaf Ronneberger, Philipp Fischer, and Thomas Brox. U-Net: Convolutional networks for biomedical image segmentation. In MICCAI, 2015.

Wenhai Wang, Zhe Chen, Xiaokang Chen, Jiannan Wu, Xizhou Zhu, Gang Zeng, Ping Luo, Tong Lu, Jie Zhou, Yu Qiao, et al. VisionLLM: large language model is also an open-ended decoder for vision-centric tasks. In NeurIPS, 2023.

XuDong Wang, Shaolun Zhang, Shufan Li, Konstantinos Kallidromitis, Kehan Li, et al. SegLLM: Multi-round reasoning segmentation. In ICLR, 2025.

Zhaoqing Wang, Yu Lu, Qiang Li, Xunqiang Tao, Yandong Guo, Mingming Gong, and Tongliang Liu. CRIS: CLIP-driven referring image segmentation. In CVPR, 2022.

Cong Wei, Yujie Zhong, Haoxian Tan, Yong Liu, Jie Hu, Dengjie Li, Zheng Zhao, and Yujiu Yang. HyperSeg: Hybrid segmentation assistant with fine-grained visual perceiver. In CVPR, 2025.

Tsung-Han Wu, Giscard Biamby, David Chan, Lisa Dunlap, Ritwik Gupta, Xudong Wang, Joseph E Gonzalez, and Trevor Darrell. See say and segment: Teaching lmms to overcome false premises. In CVPR, 2024.

Zhuofan Xia, Dongchen Han, Yizeng Han, Xuran Pan, Shiji Song, and Gao Huang. GSVA: Generalized segmentation via multimodal large language models. In CVPR, 2024.

Yuwen Xiong, Renjie Liao, Hengshuang Zhao, Rui Hu, Min Bai, Ersin Yumer, and Raquel Urtasun. UPSNet: A unified panoptic segmentation network. In CVPR, 2019.

Cilin Yan, Haochen Wang, Shilin Yan, Xiaolong Jiang, Yao Hu, Guoliang Kang, Weidi Xie, and Efstratios Gavves. VISA: Reasoning video object segmentation via large language models. In ECCV, 2024.

Senqiao Yang, Tianyuan Qu, Xin Lai, Zhuotao Tian, Bohao Peng, Shu Liu, and Jiaya Jia. LISA++: An improved baseline for reasoning segmentation with large language model. In arXiv, 2023.

Zhao Yang, Jiaqi Wang, Yansong Tang, Kai Chen, and et al. Zhao, Hengshuang. LAVT: Language-aware vision transformer for referring image segmentation. In CVPR, 2022.

Qinghao Ye, Haiyang Xu, Guohai Xu, Jiabo Ye, Ming Yan, Yiyang Zhou, Junyang Wang, Anwen Hu, et al. mPLUG-Owl: Modularization empowers large language models with multimodality. In arXiv, 2023.

Licheng Yu, Patrick Poirson, Shan Yang, Alexander C Berg, and Tamara L Berg. Modeling context in referring expressions. In ECCV, 2016.

Licheng Yu, Zhe Lin, Xiaohui Shen, Jimei Yang, Xin Lu, Mohit Bansal, and Tamara L Berg. MAttNet: Modular attention network for referring expression comprehension. In CVPR, 2018.

Shilong Zhang, Peize Sun, Shoufa Chen, Min Xiao, Wenqi Shao, Wenwei Zhang, Yu Liu, Kai Chen, et al. GPT4RoI: Instruction tuning large language model on region-of-interest. In ECCV, 2024a.

Tao Zhang, Xiangtai Li, Hao Fei, Haobo Yuan, Shengqiong Wu, Shunping Ji, Chen Change Loy, and Shuicheng Yan. Omg-LLaVA: Bridging image-level, object-level, pixel-level reasoning and understanding. In NeurIPS, 2024b.

Xiaofeng Zhang, Chen Shen, et al. From redundancy to relevance: Enhancing explainability in multimodal large language models. In NAACL, 2025.

Deyao Zhu, Jun Chen, Xiaoqian Shen, Xiang Li, and Mohamed Elhoseiny. MiniGPT-4: Enhancing vision-language understanding with advanced large language models. In ICLR, 2024.

Lanyun Zhu, Tianrun Chen, Qianxiong Xu, Xuanyi Liu, Deyi Ji, Haiyang Wu, De Wen Soh, and Jun Liu. Popen: Preference-based optimization and ensemble for lvlm-based reasoning segmentation. In CVPR, 2025.

Xueyan Zou, Zi-Yi Dou, Jianwei Yang, Zhe Gan, Linjie Li, Chunyuan Li, Xiyang Dai, Harkirat Behl, Jianfeng Wang, et al. Generalized decoding for pixel, image, and language. In CVPR, 2023a.

Xueyan Zou, Jianwei Yang, Hao Zhang, Feng Li, Linjie Li, Jianfeng Gao, and Yong Jae Lee. Segment everything everywhere all at once. In NeurIPS, 2023b.

Xueyan Zou, Jianwei Yang, Hao Zhang, Feng Li, Linjie Li, Jianfeng Wang, Lijuan Wang, and et al. Gao, Jianfeng. Segment everything everywhere all at once. In NeurIPS, 2024.

A Notations

The notations used throughout this paper are summarized in Table 14 for clarity.

Table 14: Key notations used in this paper.

Notation	Description
$\mathcal{G}_\theta$	LMMs-based segmentation model, including a multi-modal LLM $\mathcal{G}_\mathcal{T}$ and a visual backbone model $\mathcal{G}_\mathcal{V}$, $\mathcal{G}_\theta = \mathcal{G}_\mathcal{V} \circ \mathcal{G}_\mathcal{T}$
$\mathcal{H}^{(\ell)}$	the hidden states at the ℓ-th transformer layer
$\boldsymbol{h}_{t^*}^{(\ell)}$	the hidden state of `<SEG>` token at layer ℓ-th (position t^*)
$\hat{\mathbf{M}}$	the predicted binary segmentation mask
M	the ground-truth mask
M_σ	the softened label obtained by applying a Gaussian kernel to M
$\varphi(\cdot)$	a multilayer perceptron (MLP) projection layer
$\mathcal{M}_{\text{prompt}}$	mask as a prompt for SAM decoder $\mathcal{G}_\mathcal{V}^{dec}$
`<SEG>`$_{\text{prompt}}$	`<SEG>` token as prompt for SAM decoder $\mathcal{G}_\mathcal{V}^{dec}$
$\mathcal{M}_{\text{IoU}}$	the overlap between the similarity map and the ground-truth mask
$\mathcal{S}^{(\ell)}$	the similarity scores at the layer ℓ-th,
$\mathcal{M}$	the soft logit mask or similarity map $\mathcal{M} \in [0,1]^{H \times W}$
$\pi_\theta(\cdot \mid \mathcal{H}_{t^*})$	the policy distribution conditioned on $\mathcal{H}_{t^*}$
$G_\sigma(x,y)$	a 2D Gaussian kernel with σ, $G_\sigma(x,y) \propto \exp(-\frac{x^2+y^2}{2\sigma^2})$

B Discussions

B.1 Justification for Reinforcement Learning (RL)

Reinforcement Learning (RL) is introduced to address the hard-boundary problem in layer selection, enabling the model to explicitly choose a layer (*e.g.*, layer 26) in a soft, differentiable manner during training. Because hard-boundary layer selection is non-differentiable, using RL is necessary.

An intuitive approach is to train a classifier for dynamic layer selection using cross-entropy loss, followed by soft-gating via a weighted average over all layer outputs. We call this simpler alternative CE + soft-gating. Here, the layer-selection label is assigned based on the overlap (IoU) between each layer's similarity map (layers 0–31) and the ground-truth mask. The classifier is trained, and its output scores serve as soft gates to weight and fuse the transformer layers (0–31) into a unified representation, which is then fed into SAM for mask decoding. However, CE + soft-gating suffers from the following issues:

1) CE + soft-gating is numerically suboptimal. Consider a scenario after training for 1–2 epochs where the classifier predicts the following scores for layers 0–31: ($[0.01, 0.004, \ldots, 0.7, 0.1, 0.1]$). Since 0.7 is the maximum score, the 29-th layer is identified as the best layer. However, if we use the full score vector ($[0.01, 0.004, \ldots, 0.7, 0.1, 0.1]$) as soft-gating weights to fuse the embeddings of layers 0–31, the best embedding from layer 29 will inevitably be mixed with features from all other layers (0–28 and 30–31), making it no longer optimal. Soft-gating inherently prevents the remaining layers from receiving zero weight. In fact, as shown in Fig. 4 (and also discussed in (Zhang et al., 2025)), transformer layers are activated only at a few specific depths. Assigning non-zero weights to inactive layers dilutes the contribution of these key activated layers. Therefore, a hard boundary is required—that is, explicitly selecting a single layer (*e.g.*, assigning 100% weight to layer 29) rather than distributing fractional weights (*e.g.*, 60% on layer 29). This is inherently a discrete decision problem, for which reinforcement learning (RL) provides a principled and trainable solution.

2) The training objective of the layer-selection classifier (*i.e.*, CE loss) does not align with the ultimate goal of optimizing the gates through backpropagation from the downstream SAM mask decoding (*i.e.*, use soft-gating without an explicit loss on the gates). The layer-selection classifier explicitly trains the gate to predict which layer is the most important, whereas using soft weights to fuse all layers aims to optimize the averaged representation, without explicitly enforcing the gate to select the optimal layer. Besides, soft-gating presumably ignores inter-layer dependencies in the transformer. By weighting and summing all layers, it actually performs a soft ensemble, disrupting the original layer-by-layer structure of the transformer.

3) Computational cost: CE + soft gating vs. RL-gating. Given $\boldsymbol{h}_{seg} \in \mathbb{R}^{4096}$ and $\boldsymbol{h}_{img} \in \mathbb{R}^{576\times4096}$, the similarity map is computed as: $\boldsymbol{h}_{seg} \times \boldsymbol{h}_{img}^{T} = (1\times4096)\times(576\times4096)^{T} = 576$, followed by reshaping into 24×24, and then interpolating to 256×256 to obtain $\mathcal{M}$. If using the CE + soft-gating approach, one must compute the similarity map for all 32 layers of LLaVA, resulting in $32\times256\times256$ maps, and then compute the overlap (IoU) with the ground-truth mask as the supervision label. In contrast, with RL, we compute $\boldsymbol{h}_{seg}\times\boldsymbol{w}^{T} = (1\times4096)\times(32\times4096)^{T} = 32$, yielding a 32-dimensional similarity logits vector, followed by REINFORCE to select the layer index, *e.g.*, ($\ell^{*} = 28$). $\boldsymbol{w}^{T} \in \mathbb{R}^{32\times4096}$ denotes the layer-gating weights, which are the only learnable parameters in UGround. The reward r only requires computing the similarity map for a single layer.

B.2 Costs of Mask as Prompt

Compared to the <SEG> token, Mask as Prompt (MasP) is more effective, as it provides explicit spatial cues via its activation regions. Here, we analyze the computational costs associated with Mask as Prompt. We use SAM (Kirillov et al., 2023) for mask decoding. The original paper describes its prompt encoder as follows:

> *"Prompt encoder. We consider two sets of prompts: sparse (points, boxes, text) and dense (masks). We represent points and boxes by positional encodings summed with learned embeddings for each prompt type, and free-form text with an off-the-shelf text encoder from CLIP* (Radford et al., 2021)*. Dense prompts (e.g., masks) are embedded using convolutions and summed element-wise with the image embedding."*

Table 15: Mask prompt dimension changes through convolutional layers in SAM.

Layer	Output shape
Input mask: 256 × 256	(B, 1, 256, 256)
Conv2d(1 → 4, stride=2)	(B, 4, 128, 128)
Conv2d(4 → 16, stride=2)	(B, 16, 64, 64)
Conv2d(16 → 256, stride=1)	(B, 256, 64, 64)

That is, SAM accepts a mask prompt of size 256×256, which is transformed by the convolutional layers in Table 15. Thus, the final mask embedding has dimensions [B, 256, 64, 64]. In SAM's implementation, even when the mask-as-prompt input is not provided, *i.e.*, when only the text <SEG> prompt is used (`mask=None`), SAM still generates a set of learnable embeddings of the same shape as a placeholder, serving as the mask-embedding representation. Therefore, using Mask as Prompt does not introduce any additional parameter overhead.

B.3 Analogous to Monte Carlo Dropout

Analogous to Monte Carlo Dropout. Consider the query: "Can you segment the apple, orange, and banana in the picture ?" UGround responds: "Yes, apple, orange, and banana are <SEG>, <SEG>, <SEG>." That is, there are three objects to segment in a single image. During one forward pass, our SSC module (RL) selects a layer from 0–31 for each of $\texttt{<SEG>}_{apple}$, $\texttt{<SEG>}_{orange}$, and $\texttt{<SEG>}_{banana}$ as input to SAM. Suppose layers (15, 28, 19) are selected, that is, $\texttt{<SEG>}^{(15)}_{apple} \rightarrow$ SAM, $\texttt{<SEG>}^{(28)}_{orange} \rightarrow$ SAM, $\texttt{<SEG>}^{(19)}_{banana} \rightarrow$ SAM. In the ($\mathcal{T}$-1)-th forward pass, the selections are $\texttt{<SEG>}^{(16)}_{apple} \rightarrow$ SAM, $\texttt{<SEG>}^{(20)}_{orange} \rightarrow$ SAM, $\texttt{<SEG>}^{(14)}_{banana} \rightarrow$ SAM. In the $\mathcal{T}$-th forward pass, the selections are $\texttt{<SEG>}^{(13)}_{apple} \rightarrow$ SAM, $\texttt{<SEG>}^{(17)}_{orange} \rightarrow$ SAM, $\texttt{<SEG>}^{(26)}_{banana} \rightarrow$ SAM.

During the $\mathcal{T}$ forward passes, $\texttt{<SEG>}_{apple}$ from layers 15, 16, and 13 are independently connected to SAM, and the SSC module dynamically alters the model's internal connectivity. This can be analogized to the dropout mechanism in neural networks: All layers are virtually connected to SAM, but only one path is activated per forward pass. Since the SSC module performs stochastic sampling, this can be interpreted as a Monte Carlo uncertainty estimation (Gal & Ghahramani, 2016). Unlike soft-gating, the SSC module enables each layer to connect independently to SAM, resulting in 32 independent subnetworks in an ensemble-style design. As only one layer is activated at a time, the computational overhead is comparable to selecting a fixed last layer, thus avoiding expensive computational costs.

B.4 Layer-wise visualization of the Transformer

Visualization across layers 1-40. Fig. 4–6 present a qualitative analysis of similarity map activations across layers 1–40, illustrating their alignment with the ground-truth mask. Each figure contrasts heatmaps generated by prior works using a fixed last hidden layer (a) with those from our proposed Policy-Prompted Masking method (b). Unlike the baseline approach (a), our method introduces stochastic layer selection: in each forward pass, a layer ℓ^* is randomly chosen, and multiple $\mathcal{T}$ stochastic samples result in an approximate Bayesian uncertainty estimation, akin to Monte Carlo Dropout. This sampling mechanism explores diverse pathways, alleviates over-reliance on any single trajectory, and virtually forms an ensemble of subnetworks, thereby enhancing robustness. As a result, the similarity maps in (b) show activations that are sharply concentrated on the target object in intermediate and later layers, yielding more accurate alignment with the ground-truth mask compared to the diffuse and noise-prone activations observed in (a).

C Implementation Details

The UGround code repository. Currently, UGround supports 8 dataset types, namely, A: sem_seg, B: refer_seg, C: neg_refer_seg, D: correct_refer_seg, E: vqa, F: reason_seg, G: reason_seg_plus, and H: multi_reason_seg. In particular,

A: sem_seg: ade20k || cocostuff || pascal_part || paco_lvis || mapillary

B: refer_seg: refclef || refcoco || refcoco+ || refcocog || refzom || grefcoco

C: neg_refer_seg: R-refcoco || R-refcoco+ || R-refcocog

D: correct_refer_seg: fprefcoco || fprefcoco+ || fprefcocog

E: vqa: llava_instruct_150k

F: reason_seg: ReasonSeg|train

G: reason_seg_plus(LISA++): instance_seg || cot || conversations || caption

H: multi_reason_seg(muse): MultiReasonSeg|train

Our UGround is trained in a mixed fashion on these 8 types of “in-the-wild” datasets as needed. As shown in Fig. 7, the UGround project is organized with a model directory for core implementations, a scripts directory containing training and testing scripts, and a configs directory for configuration files. The main model architecture is defined in UGround.py within the UGroundForCausalLM class, which extends LlavaLlamaForCausalLM and integrates a Segment Anything Model (SAM) for mask generation. A central component of this architecture is the PolicyPromptedMasking class, detailed in PPM.py, which is instantiated and used by the UGroundForCausalLM class to dynamically select hidden state features from different network layers. The selection policy is trained using the REINFORCE algorithm with either an EMA or a critic-based baseline. All codes are provided in the supplementary material.

The UGround dashboard. As shown in Fig. 8, we developed a web-based dashboard to showcase the capabilities of UGround. The system accepts multimodal inputs, specifically a user-uploaded image paired with a natural language instruction. In response, the interface generates two outputs: (1) a segmentation mask that highlights the image region corresponding to the instruction, and (2) a textual explanation that answers the user’s query.

D Ethics and Societal Impact

Use of Large Language Models. During the preparation of this manuscript, we used Large Language Models (LLMs) primarily to aid in writing and polishing the text. Specifically, LLMs were employed for grammar correction, spelling improvements, and sentence restructuring to enhance readability and clarity. In terms of technical content, LLMs assisted only in routine tasks such as selecting tensor indices and writing dataset DataLoader code; all algorithmic ideas, methodology, and experimental designs were developed entirely by the authors. All model-generated text was reviewed and edited by the authors, who take full responsibility for the final content of this paper.

E Limitations and Future Work

We observe that UGround generally understands which object is being referred to—the semantic grounding is correct (*i.e.*, the language responses are accurate)—yet the predicted masks often fail to capture the full spatial extent of the object. The masks are frequently fragmented, perforated with holes, spatially offset, or spilled into irrelevant regions; in some cases, they even collapse entirely. This indicates that the issue does not stem from semantic misinterpretation, but from imperfect cross-modal geometric alignment.

Although the <SEG> token is intended to represent the "target object," it is fundamentally a language-space embedding whose feature distribution is not inherently aligned with the spatial structure of visual tokens. In other words, <SEG> token $\neq$ spatially aligned embedding, embedding space $\neq$ image space. For example, a distant patch of blue sky and a blue notebook on a desk may appear close in embedding space due to similar color or texture, even though they are far apart in the image. Thus, the <SEG> token captures semantic concepts rather than the spatial statistics of an object's distribution. While using the mask as a prompt does introduce spatial cues, the internal decoding mechanism of SAM remains largely unexplored, making it unclear how these cues propagate into its actual segmentation behavior.

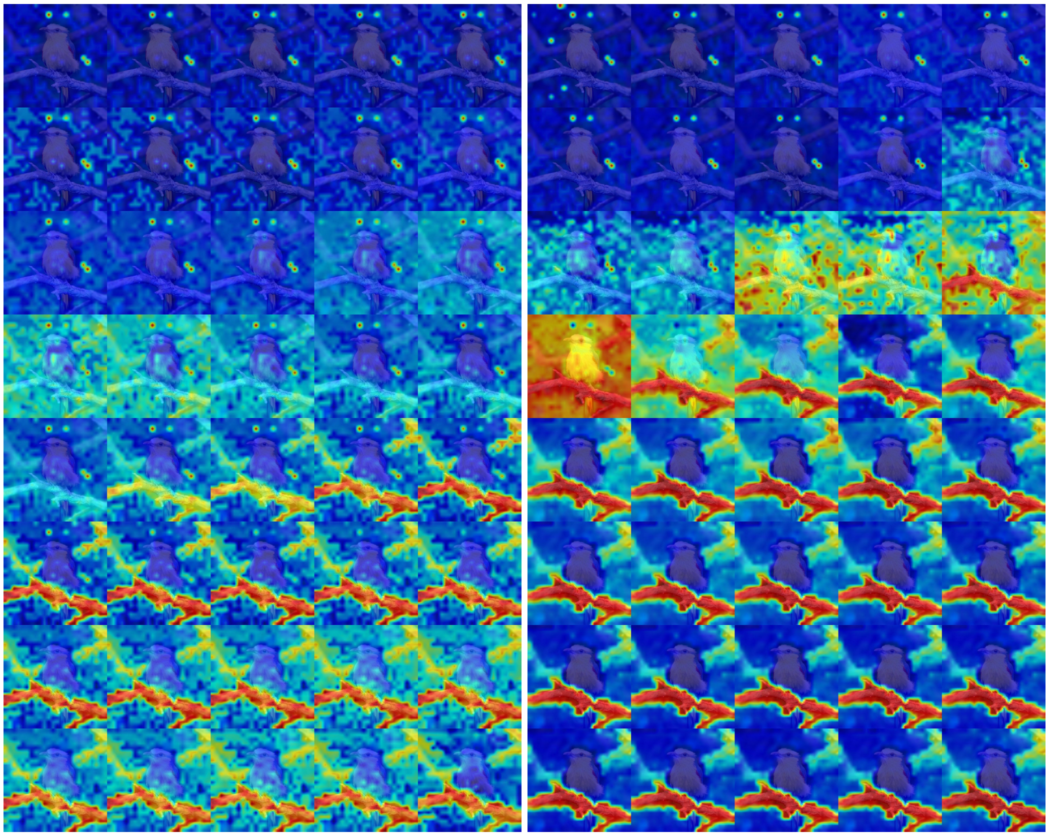

(a) Fixed last hidden layer (Prior Works).

(b) Policy-Prompted Masking (Ours).

Figure 4: Similarity map across layers 1-40.

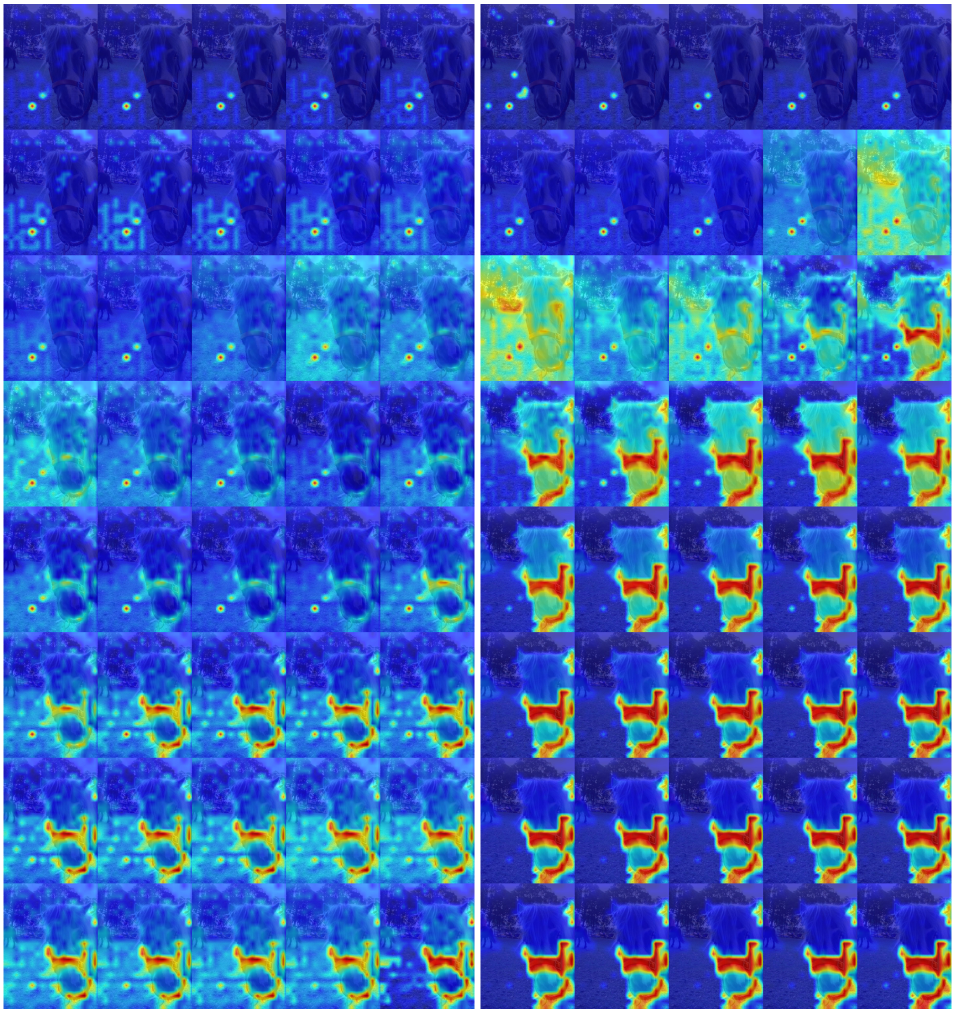

(a) Fixed last layer (Prior Works). (b) Policy-Prompted Masking (Ours).

Figure 5: Similarity map across layers 1-40.

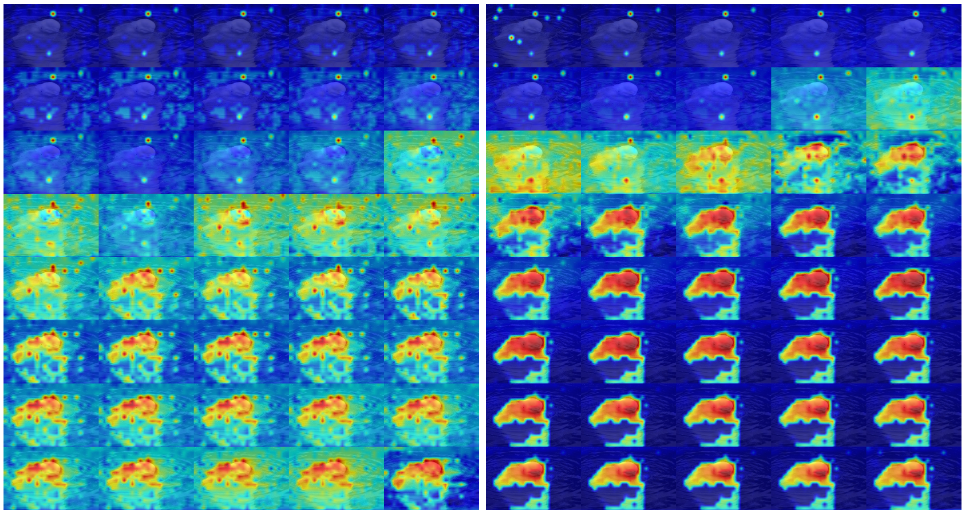

(a) Fixed last hidden layer (Prior Works). (b) Policy-Prompted Masking (Ours).

Figure 6: Similarity map across layers 1-40.

```
UGround
├──── model
│     ├──── LISA.py        ┐
│     ├──── SESAME.py      │
│     ├──── GSVA.py        ├ #Unified SOTA into a single framework
│     ├──── PixelLM.py     │
│     ├──── READ.py        ┘
│     ├──── llava
│     ├──── segment_anything
│     ├──── model_factory.py
│     ├──── PPM.py          #Our proposed Policy-Prompted Masking
│     └──── UGround.py      #Our proposed UGround
├──── scripts
├──── train_ds.py
├──── test_ds.py
├──── chat.py
├──── configs
├──── assets
├──── ...
└──── README.md
```

Figure 7: The UGround code repository.

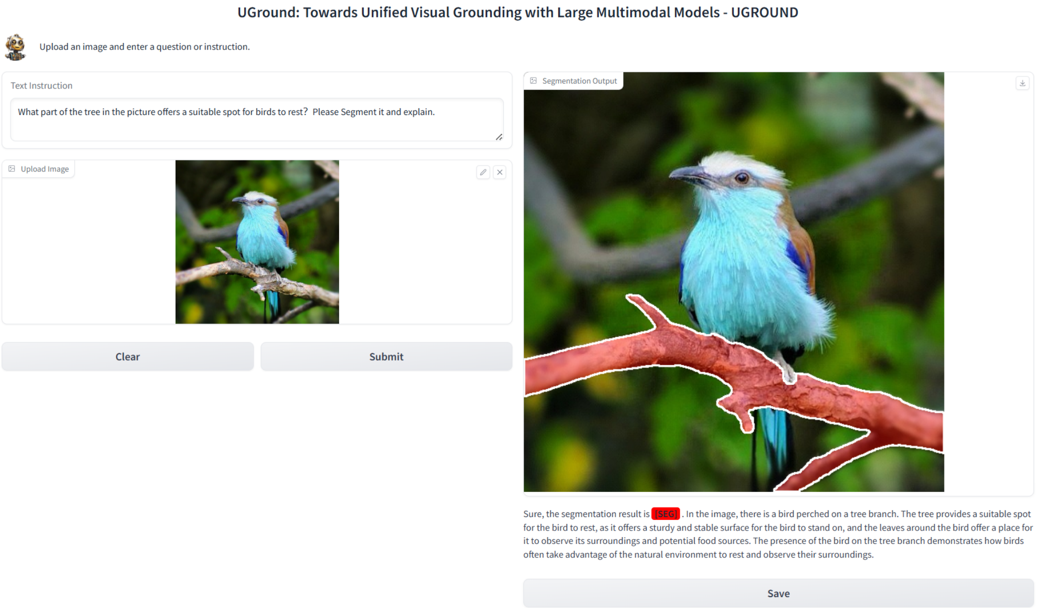

UGround: Towards Unified Visual Grounding with Large Multimodal Models - UGROUND

Upload an image and enter a question or instruction.

Text Instruction: What part of the tree in the picture offers a suitable spot for birds to rest? Please Segment it and explain.

Sure, the segmentation result is [SEG] . In the image, there is a bird perched on a tree branch. The tree provides a suitable spot for the bird to rest, as it offers a sturdy and stable surface for the bird to stand on, and the leaves around the bird offer a place for it to observe its surroundings and potential food sources. The presence of the bird on the tree branch demonstrates how birds often take advantage of the natural environment to rest and observe their surroundings.

Figure 8: The UGround dashboard.